Preprint Title	Enhanced Fuel Efficiency by Frictional Drag Reduction of Toy Boat Coated with Superhydrophobic Additives comprising Nickel Stearate and AlNiCo Nanoparticles
Authors	Kadarkaraithangam Jeyasubramanian, Silambu Selvan Paranibramma Nayagi and Gnanadhas Sobhin Osannal Hikku
Publication Date	22 Nov. 2021
Article Type	Full Research Paper
Supporting Information File 1	Supporting file.docx; 1.3 MB
ORCID® iDs	Kadarkaraithangam Jeyasubramanian - https://orcid.org/0000-0003-4300-4434; Gnanadhas Sobhin Osannal Hikku - https://orcid.org/0000-0001-8922-3603

Enhanced Fuel Efficiency by Frictional Drag Reduction of Toy Boat Coated with Superhydrophobic Additives comprising Nickel Stearate and AlNiCo Nanoparticles

Kadarkaraithangam Jeyasubramanian*[1], Silambu Selvan Paranibramma Nayagi[2], and Gnanadhas Sobhin Osannal Hikku[3]

Address:

[1]Department of Chemistry, Mepco Schlenk Engineering College, Sivakasi-626 005, Tamil Nadu, India

[2]Centre for Nanoscience and Technology, Department of Mechanical Engineering, Mepco Schlenk Engineering College, Sivakasi-626 005, Tamil Nadu, India

[3]Medical Bionanotechnology, Faculty of Allied Health Sciences, Chettinad Hospital and Research Institute, Chettinad Academy of Research and Education, Kelambakkam-603103, Tamil Nadu, India

Email: K. Jeyasubramanian (kjeya@mepcoeng.ac.in)

* Corresponding author

Abstract

Surface frictional drag developed by marine vessels utilizes a considerable percentage of fuel for propulsion. Superhydrophobic (SH) surface normally traps a layer of air at the interface and significantly reduces the surface frictional drag. Herein, the efficacy of the SH coating towards the surface drag reduction of the sailing boat is recognized by conducting a facile experiment where the bottom of the toy boat is coated with SH additives. AlNiCo nanoparticles and nickel stearate prepared by ball-milling and co-precipitation methods respectively are drop-casted layer by layer over the surface of the toy boat to impart SH. The fuel efficiency of the SH boat is improved by 51.49% substantiating the reduction in surface drag of the vessel. Further, the trapped air provides extra buoyancy force, enhancing the load-bearing capability of the SH boat by 5.77%.

Keywords

Superhydrophobicity; frictional drag reduction; fuel efficiency; AlNiCo nanoparticles; model boat.

Introduction

Natural *Nelumbo nucifera* plant leaves have micro/nanotextured nubs laminated with epicuticular wax (cuticle) which displays a high water contact angle (164º) and low sliding angle (less than 10º). For instance, while placing a droplet of water over the leaf surface, the water droplet immediately beads up and removes the dust particles on the surface and thereby, develops a clean surface and this effect opens up new fields for researchers termed as “super-hydrophobic” (SH) surfaces.[1] The nanoscale

roughened structure offers inherent hydrophobicity (WCA>90º), whereas the effective addition of low surface energy (LSE) material renovates the hydrophobic surface to the SH surface (WCA>150º). Replica of this motif is achieved by combining the nano-micro scale roughness followed by coating LSE material.[2] Such a combination introduces the non-wettable phenomenon to any desired surfaces like glass, metal, wood, paper, fabrics, etc. Owing to this inspirational phenomenon, different research methods have been developed to create a robust non-wettable superhydrophobic surface such as spin coating,[3] spray coating,[4] imprinting,[5] templating, [6] lithography,[7] plasma treatment,[8] chemical vapor deposition,[9] electrospinning,[10] etc., during the past few decades. Tu *et al.,*[11] developed the SH surface by spraying perfluoroalkyl methacrylic copolymer (PMC) suspended with TiO_2 nanoparticles (Nps) over polydimethylsiloxane precoated wood substrate, in that the TiO_2 Nps impart the essential roughness while the PMC provides LSE and binds the Nps together providing a robust coating. Alexander *et al.,*[12] functionalized aluminium oxide Nps with carboxylic acids containing highly branched hydrocarbon chains where Nps introduce roughness while carboxylic acid provides LSE resulting in a WCA of 157°. Likewise, many works of literature have proved that the Nps and LSE material can be blended to obtain a superhydrophobic surface.

Besides the self-cleaning effect, the SH effect is developed by *Aquarius remigis* (common water strider) over its leg for buoyancy effect which enables them to stand steady and move over the water surface. The buoyancy effect is introduced by the SH surface due to the air bubbles present on the interface between water and SH surface. From this nature inspiring phenomenon new idea sparks and leads to the investigation of the “floating and load-bearing” property of SH surfaces. Sun *et al.,*[13] used a novel method of constructing an aquatic robot mimicking common water strider where the legs were made of SH which carries 27.9 g (weight of robot) freely over the water

surface without sinking. The legs were made up of aluminium which was converted to SH type by acid etching followed by treatment with LSE material viz., 1H, 1H, 2H, 2H-Perfluorooctyltriethoxysilane that displays a very high WCA of 163°. Zhang *et al.,*[14] developed an aquatic robot with SH legs that freely moved and turned over the surface of the water by mimicking as that of a water strider. The SH was introduced over copper legs by a chemical etching process followed by treating with n-dodecanoic acid.

Apart from floating and load-bearing capability, the SH surface is also able to reduce the surface frictional drag on moving vessels like a boat on the water. The surface frictional drag is developed due to the frictional resistance offered by water towards the surface of moving objects. Owing to the presence of surface frictional drag, the marine moving objects such as submarines, cargo ships, steamer boats, etc. consume more amount of fuel.[15] To overcome the drawbacks, scientists have been trying to reduce the surface frictional force and thereby to enhance the fuel efficiency by employing the usage of superhydrophobic coatings. In this context, by imitating the phenomenon found in between the legs of water strider and water, it is possible to reduce the surface drag reduction. The super-hydrophobic surface reduces the surface friction through the air trapping phenomenon and the air trapped in between water and the sailing surface acts as lubricant, thereby minimizing the drag developed due to surface friction which has been validated by many researchers. Jiang *et al.,*[16] designed a grille structure of copper attached over the hull of a miniature boat made up of polyurethane foam. The copper grille was then modified with tetra decanoic acid to achieve super-hydrophobicity and the as obtained super-hydrophobic copper grille provided better drag reduction compared with the unmodified surface and thus improved the performance of the sailing boat. Wang *et al.,*[17] converted steel into superhydrophobic type by spraying PMMA suspended with nano-silica. The drag reduction displayed by

the super-hydrophobic coating was studied by sailing test and rotatory disc test to confirm the drag reduction.

All these facts have motivated us to use the superhydrophobic coating beneath a toy boat and to study its implication towards the reduction in drag and thereby pave the way for economical usage of fuel. Such a novel phenomenon was achieved by coating SH blend consisting of AlNiCo nanoparticles (prepared by ball milling process) suspended in adequate amount in the low surface energy material viz., nickel stearate. The optimized quantity of SH additive was coated on the bottom of the toy boat made of thin steel by drop casting method. The effect of the superhydrophobic coating under a toy boat was investigated through load bearing, drag reduction, and fuel consumption studies.

Results and Discussion

Characterization of AlNiCo Nps

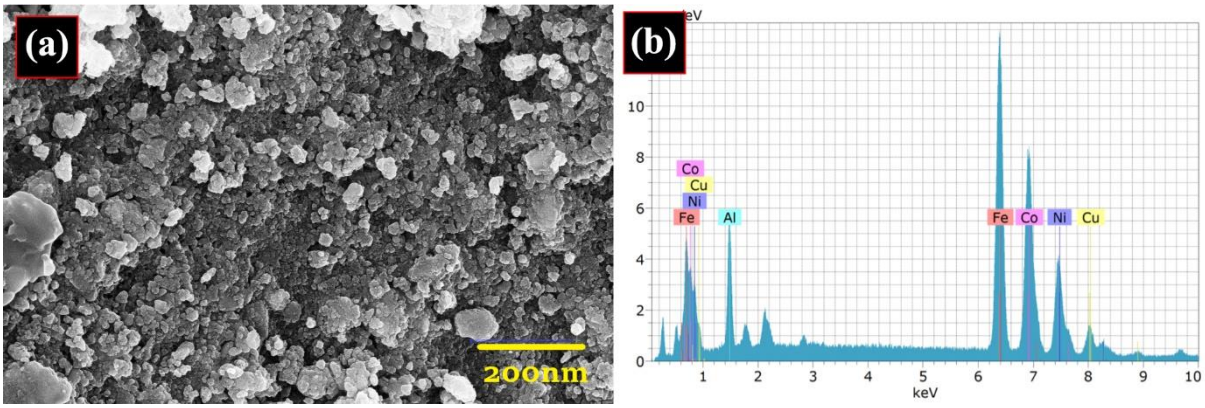

Figure 1: (a) Field emission scanning electron micrograph of AlNiCo Nps and (b) EDS spectrum of AlNiCo Nps

The FESEM image of AlNiCo Nps recorded at 50,000× magnification at a working distance of 5.7 mm is shown in Figure 1a which reveals the near spherical nature of AlNiCo Nps throughout the sample size. The EDX spectrum shown in Figure 1b directly

establishes the existence of elemental composition such as aluminium, nickel, cobalt, iron, and copper with a trace amount of oxygen. Even though the AlNiCo Nps is milled in an argon atmosphere; the oxygen peak is originated owing to the formation of oxides in trace amount.

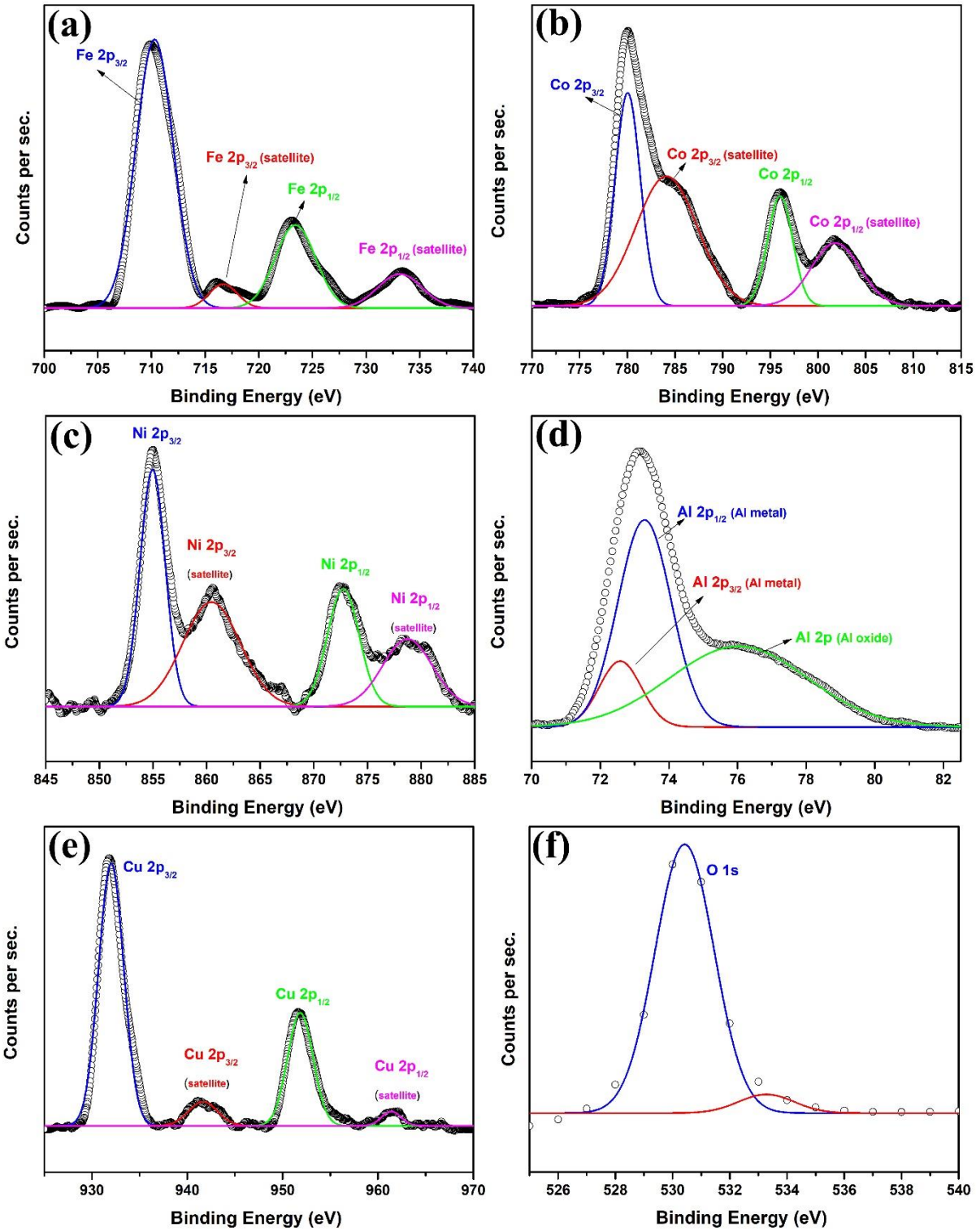

Figure 2: XPS spectra of (a) iron, (b) cobalt, (c) nickel, (d) aluminium, (e) copper & (f) oxygen

Figure 2 brings the sight of high-resolution photoelectron peaks about the 2p spin-orbit splitting level of Al, Ni, Co, Fe, Cu and the 1s spin-orbit level of O. The broadened peak at 723.29 eV and 710.02 eV of Fe shown in Figure 2a constitutes for $2p^{1/2}$ and $2p^{3/2}$ spin-orbit splitting.[18] The bifurcation of 15.58 eV peak of 2p spin-orbit splitting of Cobalt is $2p^{1/2}$ and $2p^{3/2}$ found at 796.22 eV, 780.64 eV is shown in Figure 2b.[19] The binding energy separation of 17.7 eV attributable to the peaks appearing at 872.79 eV and 855.095 eV is consistent with Nickel [Figure 2c].[20] Figure 2d reveals the deconvoluted photoelectron peaks of Al corresponding to $2p^{1/2}$ and $2p^{3/2}$ with the binding energy of 73.34 eV & 67.19 eV.[21] The 2p doublet peak appearing at 951.86 eV and 931.91 eV of copper well matches the literature and is shown in Figure 2e with 19.95 eV separation.[22] The adventitious O1s singlet peaks are found at 530.98 eV[23] and displayed in Figure 2f. The presence of oxygen facilitates metal oxide formation during the ball milling process.

Characterization of AlNiCo Nps

The AlNiCo Nps are first made to coat over steel substrate followed by functionalization with nickel stearate and subjected for characterization. Figures 3a&b show the FTIR spectra recorded in the wave number range from 500 cm^{-1} to 4000 cm^{-1} at room temperature. Figure 3a is the FTIR of nickel stearate that displays no peak near 3500 cm^{-1} (-OH) confirming the efficient conversion from $Ni(OH)_2$ to $C_{36}H_{70}O_4Ni$. The peaks found at 2849 cm^{-1} and 2910 cm^{-1} attributed to the symmetric and asymmetric vibrations of the aliphatic $-CH_2-$ group originate from stearate.[24] The peak corresponding to -COOH appearing at 1698 cm^{-1} confirms the presence of excess stearic acid which adheres to the surface of nickel stearate.[24] The emergence of two

peaks at 1414 cm^{-1} and 1558 cm^{-1} is due to the formation of -COO- group, here it is possibly –COONi.[25] However, while adding nickel stearate to AlNiCo Nps a noteworthy feature is noticed where the peak intensities of 1414 cm^{-1} and 1558 cm^{-1} increase and the peak at 1698 cm^{-1} reduces [Figure 3b]. This is due to the conversion of -COOH into -COO- in the presence of the metal moiety such as Al, Ni, Co, and Fe confirming the formation of metallic stearates. The occurrence of this phenomenon is facilitated by the free-standing stearic acid. All these facts elucidate the fact that there exists a healthy adherence of nickel stearate with AlNiCo Nps.

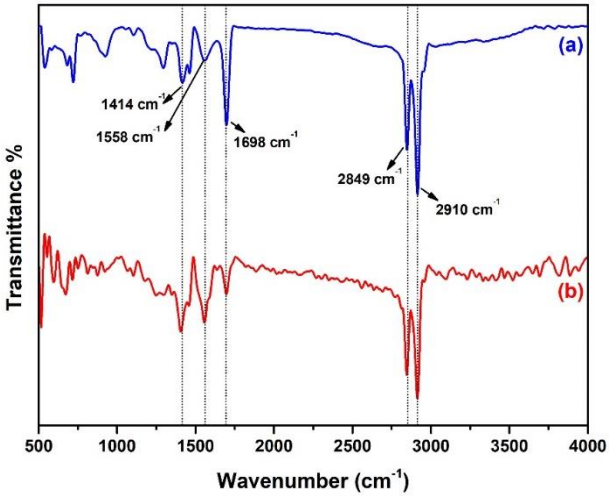

Figure 3: FTIR spectra of (a) nickel stearate and (b) AlNiCo Nps coated with nickel stearate

Figures 4a-d is the 3D AFM images of bare steel, AlNiCo Nps, nickel stearate and nickel stearate over headed AlNiCo Nps coated steel specimen recorded in the scan range of 2.5×2.5 µm in a non-contact mode. The topography of the polished steel specimen appearing like a smooth surface does not have any appreciable peaks and valleys as shown in Figure 4a. Figure 4b is the image explored after placing AlNiCo Nps. The particles are layered over the steel and show up a well-organized arrangement of particles in a layer like structure having a height of 400-600 nm. The AFM image of the nickel stearate coated steel substrate is shown in Figure 4c, which

shows particles with a size of 250 nm. The composite film consisting of both AlNiCo Nps and nickel stearate coated over steel appears like a textured surface [Figure 4d], in which the components are packed with height upto 800 nm. The wet nature of the coated surfaces is mainly influenced by the surface roughness of AlNiCo Nps and subsequently coated with the low surface energy nickel stearate. Rough nature developed by AlNiCo Nps, nickel stearate film and their blend can be assessed by evaluating the surface roughness by line profile analysis using XEI software. The 2D images of uncoated steel, steel coated with AlNiCo Nps, nickel stearate coated specimen and the composite coated steel are shown in supplementary information [Figures S1a-d]. Using the software, over the 2D image of the specimen scanned in the chosen area, vertical and horizontal lines are drawn which pass vertically and across the coating on the steel. Based on the line that passes over the peaks and valleys on the selected portion, the roughness parameters can be obtained. The details related to the line drawn on various images on the x-axis (vertical line) and y-axis (horizontal line), the average roughness (Ra), the maximum height of the roughness profile (Rz), and the root mean square roughness (Rq) are given in Table 1.

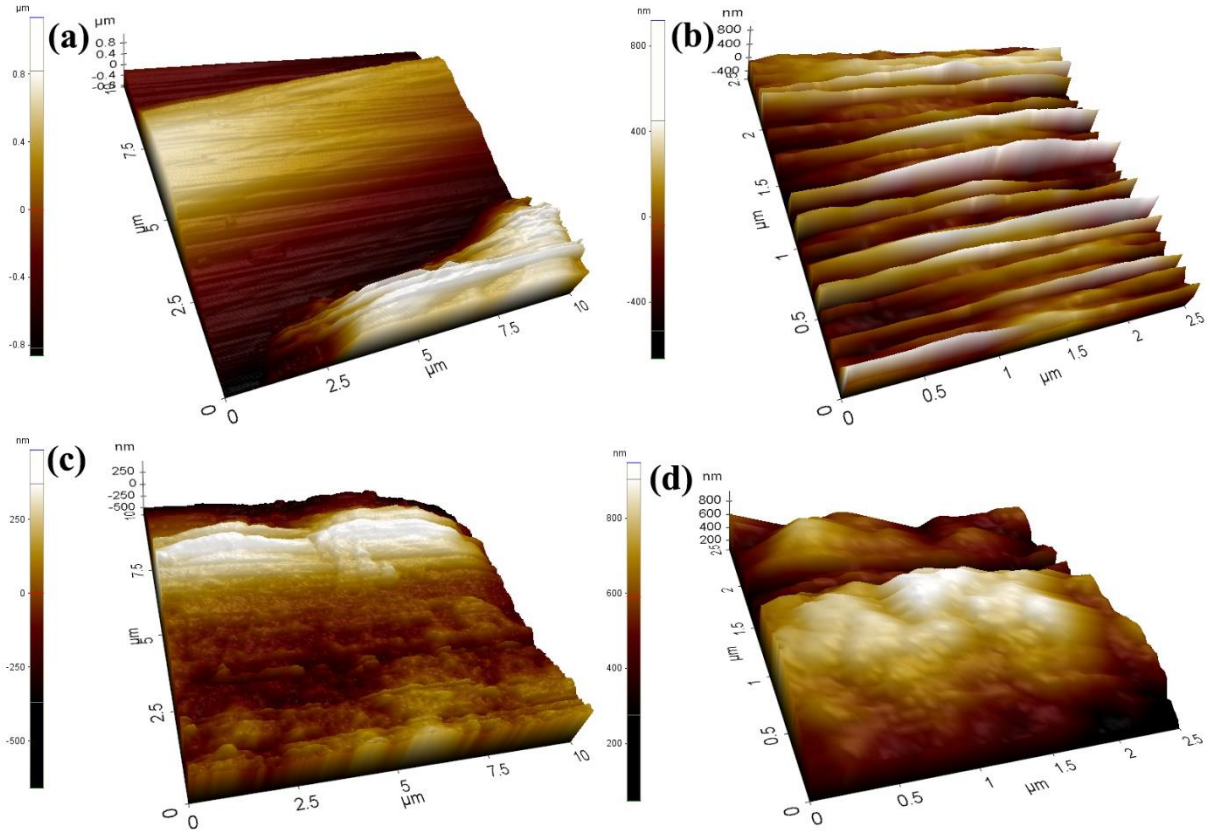

Figure 4: 3D AFM image of (a) bare steel (b) AlNiCo nanoparticles (c) nickel stearate film and (d) composite film having both AlNiCo & nickel stearate

Table 1: AFM Line profile data analysis of prepared samples

Sl. No.	Specimen	Roughness (nm)					
		Ra		Rz		Rq	
		x-axis	y-axis	x-axis	y-axis	x-axis	y-axis
1	Bare steel	374	237	1194	715	414	273
2	AlNiCo coated steel	379	482	1864	1485	461	527
3	Nickel stearate coated steel	167.95	122.75	645.69	366.88	208.68	134.89
4	Composite coated steel	633	711	2295	1438	712	792

From the table, the Ra found on the composite coating is high (711 nm), which is one of the prerequisites needed for a coating, which can mimic the natural lotus leaves. The submicron level roughness of 0.752 µm existing in the coating combined with low

surface energy material satisfies the Cassie-Baxter state of a non-wettable substrate and enhances the WCA of bare steel from 72° to 153.4°.

Superhydrophobic surfaces being designated depend on the wetting behavior where the surface should have a contact angle exceeding 150°. The surface that has higher WCA obeys Cassie-Baxter's equation

$$Cos\,\theta c = f_1 Cos\theta_1 + f_2 Cos\theta_2 \quad (1)$$

where θc is apparent contact angle, f_1 is the surface fractions of the liquid-solid interface, f_2 is the surface fractions of the liquid-air interface in which the air pockets are filled within the grooves pertinent to the wetting of a textured surface of a composite or heterogeneous state.[26] In the present case, owing to the large surface roughness, the air can be easily trapped in between the grooves which results in super-hydrophobicity. Super-hydrophobicity of the AlNiCo Nps coated surface is examined by measuring the WCA using the goniometer. The water droplet of 5 µl is dispensed by a 500 µl gas tight precision syringe and dropped at a speed of 0.10 µL/s. The sample stage is moved with the specimen in an upward direction until the drop settles down on the sample. The image of the water droplet being placed on the substrate is snapped using a USB 2.0 wide-VGA camera, and the WCA determined through the SCA20 software is shown in Figure 5.

The WCA of the bare steel is about 72° [Figure 5a]; this shows that the metallic substrate gets easily wetted due to the hydrophilic nature of steel having an affinity towards the polar solvent. This affinity is generated due to the difference in surface energy of steel substrate and water. The surface energy of iron (the main constituent of steel) is 2525 dynes/cm, whereas it is 72.8 dynes/cm for water. On damping with a droplet of water on a steel specimen coated with nickel stearate alone exhibits the WCA as 113.6° [Figure 5b], the improvement in WCA of steel after coating with nickel stearate is attributed to the reduction in surface energy of steel by stearate molecules.

Even though the surface energy is reduced the surface doesn't display super-hydrophobicity. This is because the surface does not have the necessary roughness. Figure 5c is the WCA image of water drop after being dropped over the steel substrate coated with 0.0125 g of AlNiCo Nps. The WCA reveals a very least value of 23° attributed to its hydrophilic nature and the strong adherence nature of AlNiCo Nps with steel which influences the higher wetting tendency of water droplets. While mixing the AlNiCo Nps with nickel stearate in the ratio 5:4, the WCA is found to be enhanced (153.4°) and validates [Figure 5d] the super-hydrophobic nature. The WCA values of nickel stearate and AlNiCo Nps separately coated over steel substrate do not display super-hydrophobicity. However, blending AlNiCo Nps with nickel stearate enhances the WCA to superhydrophobic type which is attributed to the synergistic effect of both the low surface energetic nature of nickel stearate and the roughness enhancing tendency of AlNiCo Nps.

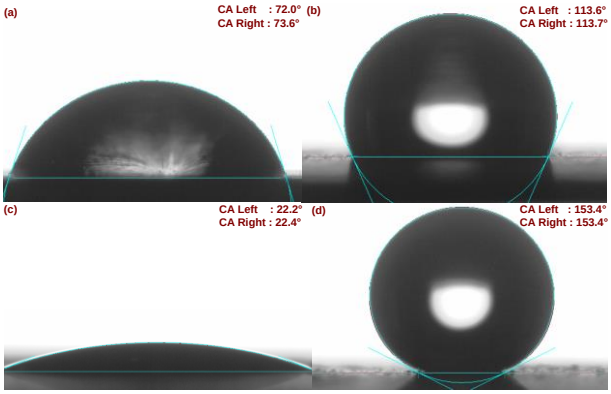

Figure 5: WCA of (a) bare steel (b) nickel stearate coated steel (c) AlNiCo Nps coated steel and (d) nickel stearate over headed AlNiCo Nps coated steel

Further, the advancing and receding contact angles of the prepared super hydrophobic surface are measured using Needle method. The needle is brought close to the substrate surface and water is continuously dispensed slowly (0.01 µl/s) till the final volume of 3 µl droplet is reached. When the contact between the substrate and the droplet is increasing, the WCA is measured as 156.08° denoting the advancing angle

[Figure 6a]. Then, the droplet is sucked slowly off the substrate and consequently, the contact line withdraws where the receding contact angle is measured as 153.25° [Figure 6b]. The hysteresis is quantified by calculating the difference between the advancing and receding contact angle as 2.83°.

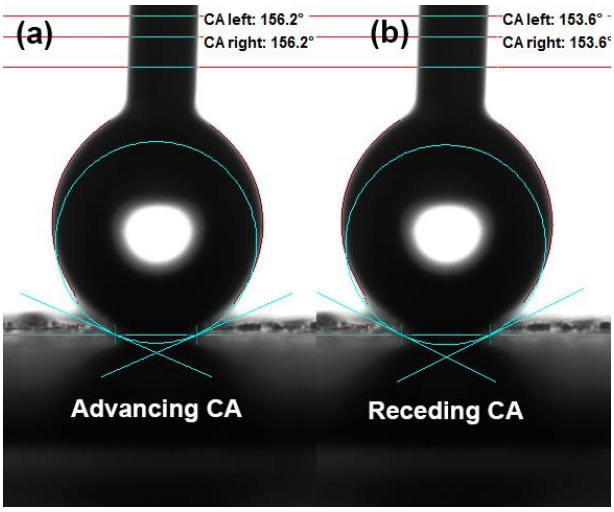

Figure 6: (a) Advancing and (b) receding contact angle of SH surface

Floating nature of the superhydrophobic surface

The floatation and the immersion of an object depend predominantly on the buoyant force which depends on the density, shape, volume, porosity, etc., of the object. If the buoyant force is less than the weight of the object, the object will sink in water, whereas if the buoyant force is higher than the object's weight, it will float. For instance, a steel boat will float (upthrust) whilst a steel plate will sink [Figure 7a] which is influenced by the shape of the object that has a direct impact on the displacement of the water.

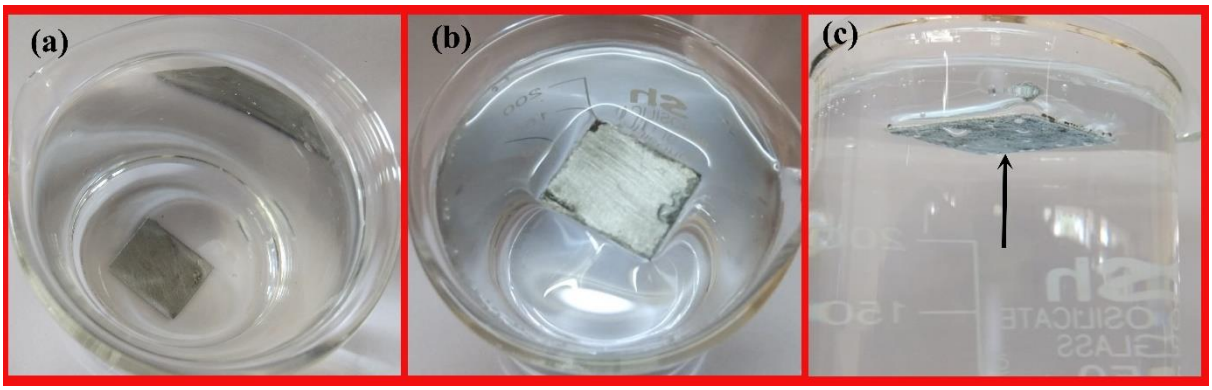

Figure 7: Photographic image of (a) steel plate sinking in water (uncoated), (b) floating nature of superhydrophobic steel and (c) air bubbles formed at the solid-liquid interface

All these facts are explained by Archimedes in terms of the prominent law of buoyancy. Some of the denser bioengineering species found in nature like *Gerris lacustris* slide on water owing to its hierarchical conical-shaped tapered micro setae which have longitudinal and quasi-helicoidal nano groves that help them to float and move freely over the surface of water. Based on the Cassie-Baxter equation $\text{Cos}\ \theta_1 = f_1\ \text{Cos}\ \theta_w - f_2$, the f_1 is the surface fraction of micro setae with nano grooves, f_2 is the surface fraction of air on the leg surface and θ_w is the contact angle of the wax secreted by the water strider. The air pockets filled in the spaces between the micro setae and nano grooves prevent the leg from being wet. Such natural floating magic is used to evolve several floating objects employing superhydrophobic coatings. Intending to check the floating nature of the superhydrophobic surface, nickel stearate over headed AlNiCo Nps coated steel possessing a high water contact angle (153.4°) is placed over water. Figure 7b shows the floating ability of the superhydrophobic mixture coated side of steel (2×2 cm) whose density is abundantly greater than water. The superhydrophobic coating of the steel substrate repels water and the air bubbles formed at the solid-liquid interface prevent the substrate from being wetted and influence the buoyant nature as shown in Figure 7c. The buoyancy nature and the load bearing ability of the steel substrate coated with superhydrophobic additives are supported by the factors like curvature force, air bubbles present across the interface (plastron), etc.

Load bearing of a superhydrophobic miniature boat

Besides the floating ability, the non-wettable substrate is also able to bear additional loads being placed on the floated substrate without any disturbance. AlNiCo-nickel stearate coated steel is capable of supporting the additional weight of 0.3136 g

(estimated by keeping more stapler pins over the substrate) along with the steel weight (3.28 g) and is shown in Figure S2. *Gerris lacustris* may stand and quickly slide over the surface of water due to its legs and surface tension of water. The surface tension of water creates a membrane around the legs and it gives support by 15 times the total weight of the insect to stand. Mimicking the natural living being like *Gerris lacustris*, a freely floated non-wettable substrate that can be quickly propelled over the surface of water satisfies the following conditions: The surface must be superhydrophobic (to prevent the penetration of water and cohesion with the free surface) and should have lightweight to reside over the surface of the water.[27] Inspired by this phenomenon, the bottom area of the steamer toy boat is coated with AlNiCo nanocoating and over headed with nickel stearate as shown in Figures S3a&b which is named as the superhydrophobic miniature boat (SHM), while the uncoated steamer boat is a hydrophilic miniature boat (HpM). After floating the boats on water [Figure S3c], the load-bearing nature is evaluated by placing Indian Rupee coins in an increasing number separately on SHM and HpM boats in the floating condition. SHM boat displays an ultimate load-bearing capacity of 69.6 g, whereas the HpM boat is able to bear only 65.8 g which is 5.46% less than the load supported by the SHM boat [Figures S3d&e].

Drag reduction of superhydrophobic miniature boat

To study the drag reduction phenomenon of the non-wettable and the wettable substrate, the SHM boat and the HpM boat are propelled by burning 0.5 ml of gingelly oil (0.4471 g) with 0.0108 g of cotton wick having the calorific value of 15.43 kJ/g taken in a scoop (1.4146 g) placed inside the boat. The copper steam chamber is connected to two metallic pipes whose ends are opened at the back end of the boat. 1.6 ml of water is taken in a syringe and carefully injected into one end of the metallic pipe until water comes out through the second pipe. After lighting the wick, steam produced

escapes from the steam chamber and propels the boat in the forward direction. In both cases, the boats are allowed to run over water till the complete utilization of 0.5 ml oil which is loaded initially. After complete burning of fuel, the total distance traveled by the boats and the time taken to cover the distance are measured. The SHM boat ran over water for 700 s and traveled a distance of 99.62 m. The distance covered by the boat is measured from the distance of the periphery of the vessel holding water (1.542 m). In 700 s, the boat runs for about 64 cycles and 93.2 cm of 65^{th} cycle, the distance covered by the boat is calculated as (64 × 154.2 + 93.2) as 99.62 m. The same strategy is adopted to evaluate the distance traveled by the HpM boat employing 0.5 ml of oil as fuel. In this case, the boat traveled over water for about 525 s and completed 42 cycles and 100.2 cm of 43^{rd} cycle from which the total distance traveled by the boat is computed as (42 × 154.2 + 100.2) 65.76 m. The difference in time and the distance traveled by the boats are correlated to the drag reduction nature of the non-wettable coating. In the case of SHM coated boat, the water molecules do not have any sticking tendency owing to the presence of air molecules in between the water-repellent coating and water which minimizes the frictional force. Due to this fact, the toy boat travels a distance of 99.62 m in 700 s. In contrast to SHM, HpM is a conventional type, sticking firmly with water molecules, and has its own frictional resistance. So, the HpM boat travels only 65.76 m in 525 s. The average speed of HpM and SHM boats is calculated from the ratio of distance covered by the boat to the time taken as 0.1253 m/s and 0.1423 m/s respectively.

Usually, the interaction of water with the surface of the moving object produces friction which causes the drag of the boat. It has been reported that more than 50% of the fuel is utilized by marine vehicles to overcome the drag developed due to the friction. Thus, reducing the frictional drag can effectively improve fuel efficiency which is a global concern. It has been already reported that the super-hydrophobic surfaces have the

ability to reduce drag reduction. When the super-hydrophobic surface is made to float over water, there forms an air gap between the solid substrate surface and water molecules. This can be very well understood from Figure 7c where air bubbles can be observed between the solid and the liquid interface. Therefore, the solid-liquid interface (conventional case) is altered to solid-air-liquid interface (substrate modified to super-hydrophobic type). Hence, the friction (f_{sl}) due to the solid-liquid interface is split to solid-gas friction (f_{sg}) and liquid-gas friction (f_{lg}). However, f_{sg} and f_{lg} are much lower than the f_{sl} resulting in the reduction in frictional resistance.[15] This reduction in friction is caused due to the air trapped in between the interface where water can be moved with ease than unmodified surfaces. Even though, there are literature that stated about the increase in drag because of SH surfaces, the drag is occurred due to the adhesive force of water with the SH surfaces.[28; 29] The adhesive force leads to the coverage of water in the grooves of SH surface leading to additional drag. However, this whole phenomenon completely relies on the SH coating properties. In the present case, the adhesion force is limited leading to better fuel efficiency and improved propulsion of the SHM boat than HpM boat. In-directly, this adhesion force can be determined by WCA of the surface; more specifically, by the receding contact angle of the SH surface. Receding contact angle is the critical contact angle below which the solid-liquid-gas contact line retraction is initiated and therefore, SH surface with larger receding contact angle exhibits lower adhesion force. In the case of AlNiCo coated superhydrophobic surface, the receding contact angle is measured as 153.25° validating the low adhesive force of SH surface. When the sample is directed towards and touches the droplet present at the tip of the needle, the water droplet is not easily dropped down over the substrate but sticks to the needle instead owing to the low adhesion force of the SH surface. Consequently, the frictional force between the SH surface and water is limited in the case of SHM boat leading to drag reduction due to the plastron effect. From

these facts, it is evident that the SHM boat moves faster over water and reaches the destination in a shorter duration owing to the non-wettable coating applied on the bottom. Besides, the efficacy of the coating towards saving fuel is explained as follows: The difference in speed over water by SHM and HpM boats ensures that the drag reduction is the combined function of the driving force of the propelled boat and the frictional force acting over the boats.[30] The driving force acting on the SHM boat is increased as a result of the non-wettable bottom area and the air bubbles present at the interface facilitate the movement of the SHM boat in the forward direction easily. But in the case of the HpM boat, owing to the absence of these two features, it travels slowly. The slow motion of the HpM boat compared with SHM is justified using the optical images of boats riding over the water tub [Figures 8a&b]. From Figure 8, it is clear that after 16 sec SHM boat has covered 2 complete cycles. However, the HpM boat travels only ~1.33 cycles showing the effective drag reduction in the SHM boat. Even though the trajectory of the boat is not straight, it does not affect the drag reduction phenomenon of the SHM boat. This implies that the Cassie-Baxter state is not converted in to Wenzel state even with the disturbances facilitated by the curved path.

Figure 8: Photographic images of (a) HpM boat and (b) SHM boat at different interval (images are taken from the second cycle of travel for both the boats)

All these facts are more useful in the validation of fuel saved in the case of SHM boat than the HpM boat. From the distance traveled by SHM and HpM boats, it is evident

that the HpM boat runs over water using 17.44 kJ/g energy as fuel and travels a distance of 65.76 m in 525 s with an average speed of 0.1253 m/s. At the same time, the toy boat coated with superhydrophobic coating covers the same distance in 403s and uses only 11.11 kJ/g of fuel. While comparing the energy used by the boats for traveling the distance of 65.76 m, the SHM boat uses only 11.11 kJ/g, whereas the HpM boat utilizes about 17.44 kJ/g (calculations are provided in supporting information, S4). The difference in energy, i.e. 6.33 kJ/g is saved in the case of the SHM boat in contrast to the HpM boat. The difference in energy conserved by the SHM boat is equal to 0.1623 g of fuel in contrast to the boat which does not have water repellent coating. Further, from the distance traveled by the toy boats (SHM and HpM), the SHM boat travels about 51.49% more distance than the HpM boat on using the same quantity of fuel. All these results reveal that the boat coated with non-wettable coating possesses remarkable drag reduction nature and saves fuel economically. Further, it can be effectively used in aquatic devices in the future.

Conclusion

The air trapping phenomenon of superhydrophobic surfaces, when immersed in water, can be effectively utilized to reduce the frictional drag resistance of moving vessels in water as well as for reducing fuel consumption. In this work, the successful achievement of non-wettability on the steel basement of a toy boat is done by coating superhydrophobic additives employing AlNiCo Nps and nickel stearate. Superhydrophobic WCA of 153.4º is attained by mixing AlNiCo nanoparticle (surface roughening agent) and nickel stearate (low surface energy material). The superhydrophobic boat is able to bear 69.6 g of load, whereas the unmodified boat has the capability to carry 65.8 g substantiating the improvement in load bearing capability.

The toy boat coated with superhydrophobic additive travels a distance of 99.62 m in 700 s using 0.4471 g of gingelly oil as fuel, whereas the toy boat which is not coated with any material traveled only 65.76 m in 525 s by consuming the same quantity of fuel. In comparison with the HpM boat, the SHM boat travels about 51.49% extra distance and saves 6.33 kJ/g of the fuel during the running in 525 s. From this study, it is understood that the surface modified boat travels more time than the uncoated boat which is supported by the drag reduction phenomenon, which is facilitated by the synergistic effect of water repellent nature and the occluded air molecules in between the toy boat and water surface. This pilot scale study indicates that coating super-hydrophobic mixture by a simple drop-casting technique can effectively improve the fuel efficiency of moving objects over liquid. In future, the development of Super-hydrophobic paint with high corrosion resistance will not only protect it from corrosion but also save fuel to a considerable extent.

Materials and Methods

Materials

Metallic powders, used in this work, like cobalt (Loba chemical, 99.5%), nickel (Sisco research laboratories, 99.5%), aluminium (Reachem, 99.5%), iron (Loba chemical, 99.5%), copper (Loba chemical, 99.5%), and the chemicals like sodium hydroxide (Merck, 99.9%), nickel chloride (Merck, 99.9%), stearic acid (SD fine chemical limited, 99%), methanol (Loba chemical,99.5%), toluene (Merck, 99.9%) were purchased and used without any further purification process.

Preparation of nickel stearate ($C_{36}H_{70}O_4Ni$)

4.7767 g of nickel chloride and 0.9488 g of sodium hydroxide were dissolved in 20 ml distilled water separately and mixed together gradually by adding in a drop wise manner. Instantly, a glassy green solution formed turned into an emerald green color precipitate which indicated the formation of nickel hydroxide [Reaction 1]. Then the solution was kept in a water bath at 60°C for 1 h. The supernatant solution was decanted and then the precipitate was thoroughly washed in distilled water for 4 times and filtered. Meanwhile, 5.68 g of stearic acid was dissolved in 100 ml distilled water by heating on a hotplate at 90°C for 10 min under constant stirring. After the complete dissolution of stearic acid, the nickel hydroxide precipitate was added slowly into the stearic acid solution with constant stirring. After 10 min, the green colored nickel stearate particles that were obtained floated on the surface and they were collected via filtration, washed several times using distilled water and dried in a hot air oven at 60°C for 12 h and stored in vacuum [Reaction 2].

$$NiCl_2 + 2NaOH \rightarrow Ni(OH)_2 + 2NaCl \quad \text{(R1)}$$

$$Ni(OH)_2 + 2CH_3(CH_2)_{16}COOH \rightarrow Ni(CH_3(CH_2)_{16}COO)_2 + 2H_2O \quad \text{(R2)}$$

Preparation of AlNiCo Nps

AlNiCo Nps were obtained by milling the precursor elemental metal powders like aluminium-10%, nickel-18%, cobalt-30%, iron-40% and copper-2% (planetary mono mill pulverisette 6, Germany). Toluene was added as a process control agent to prevent agglomeration during milling where the ball to powder ratio was maintained at 10:1. Argon gas was passed at 1m bar pressure for 5 min through the lid before milling to maintain inert atmosphere.[31] Then the metal powders were pulverized at 300 rpm for 30 h. During milling, argon gas was admitted periodically once in 30min to exclude

the contact of air during milling and toluene was introduced to maintain wet conditions throughout the milling process.

Preparation of super-hydrophobic coating

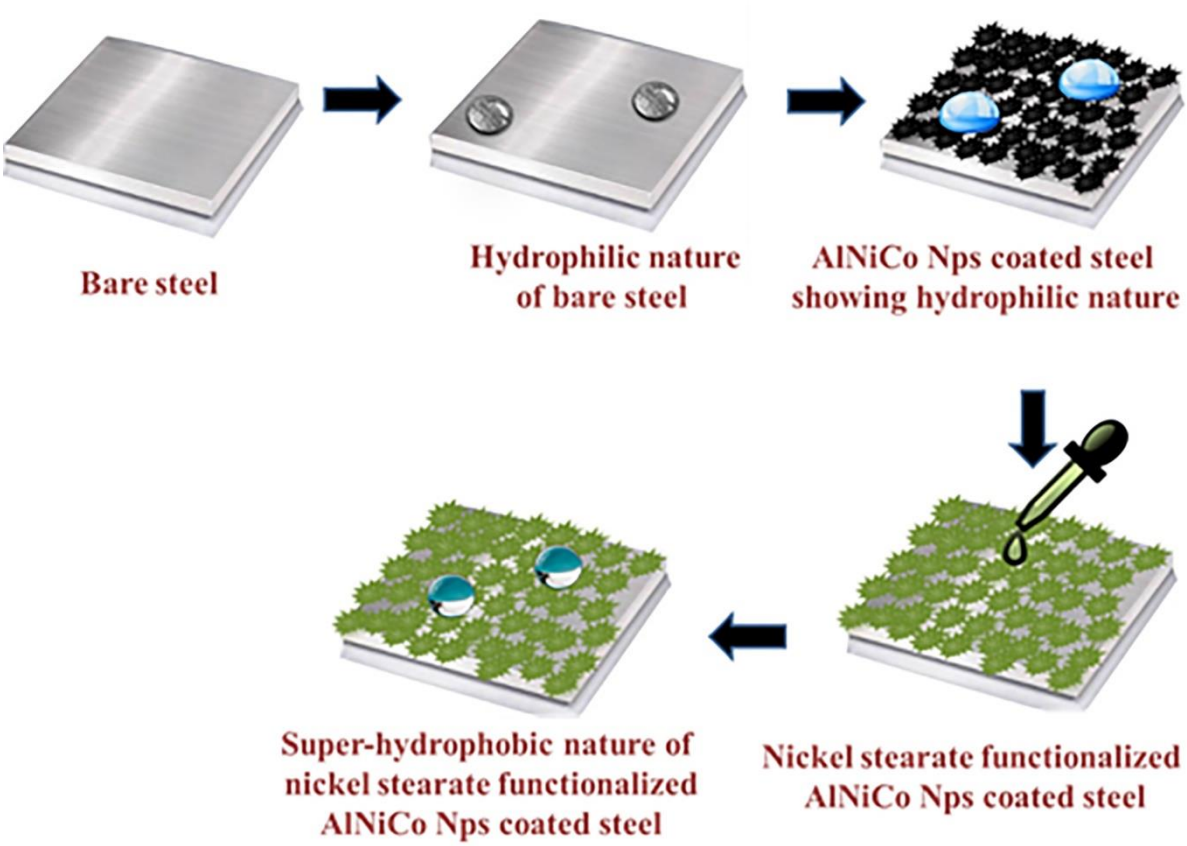

Scheme 1: Procedure for developing superhydrophobic surface

A steel plate of size 7.5 × 2.5 cm with a thickness of 0.045 cm was cleaned by crocus cloth, degreased with a copious amount of acetone and ethanol. 0.0125 g of AlNiCo Nps was dispersed in 50 ml toluene followed by ultrasound irradiation for an hour using probe type sonicating (Sonics-VCX600-USA) with Ti horn. The resultant suspension consisting of AlNiCo Nps was drop casted over the substrate which produced a uniform coating over steel. Over the AlNiCo Nps coated substrate, 0.005 g/ml nickel stearate solution was drop casted uniformly. While the solvent was evaporating, a coating of nickel stearate was given over AlNiCo Nps. The schematic representation of coating

is provided in Scheme 1. Further, the same quantities of AlNiCo Nps and nickel stearate were coated individually over other steel substrates for comparison.

Characterization techniques

Morphology of the AlNiCo Nps was recorded using Field Emission Scanning Electron Microscope (FESEM, Carl Zeiss microscopy ltd, Germany) operated at an acceleration voltage of 10 kV attached with an Energy dispersive X-ray (EDX) analyzer. The chemical state, electronic state, and binding energy of the elements present in AlNiCo Nps were scrutinized from the X-ray photoelectron spectroscopy spectra (Physical Electronics, model- PHI 5000 versa probe III). The molecular vibrations that exist in nickel stearate and nickel stearate over headed AlNiCo Nps were analyzed through Fourier transform infrared spectroscopic spectra recorded with Bruker optics, Alpha model, Germany. The surface topographies and WCA of the steel substrates before and after modification were analyzed through Atomic Force Microscope (AFM, XE-70, South Korea) and goniometer (OCA15EC, Dataphysics Instruments, Germany) respectively.

Acknowledgements

Authors would like to thank the Management and the Principal of Mepco Schlenk Engineering College for their constant encouragement and support.

Funding

No funding received

References

[1] J. Zha, N. Batisse, D. Claves, M. Dubois, *Journal of colloid and interface science*. **2019**, *553*.
[2] M. Khodaei, S. Shadmani, *Surface and Coatings Technology*. **2019**, *374*.
[3] S. Zhai, H. Zhao, *Applied Physics Letters*. **2019**, *114*.
[4] S. M. Gateman, K. Page, I. Halimi, A. R. C. Nascimento, S. Savoie, R. Schulz, C. Moreau, I. P. Parkin, J. Mauzeroll, *ACS applied materials & interfaces*. **2019**, *12*.
[5] I. Y. Moon, B. H. Kim, H. W. Lee, Y.-S. Oh, J. H. Kim, S.-H. Kang, *International Journal of Precision Engineering and Manufacturing-Green Technology*. **2020**, *7*.
[6] Y. Qing, C. Long, K. An, C. Hu, C. Liu, *Journal of colloid and interface science*. **2019**, *548*.
[7] L. Dong, Z. Zhang, R. Ding, L. Wang, M. Liu, Z. Weng, Z. Wang, D. Li, *Surface and Coatings Technology*. **2019**, *372*.
[8] J. Yang, Y. Pu, H. He, R. Cao, D. Miao, X. Ning, *Cellulose*. **2019**, *26*.
[9] A. Tombesi, S. Li, S. Sathasivam, K. Page, F. L. Heale, C. Pettinari, C. J. Carmalt, I. P. Parkin, *Scientific reports*. **2019**, *9*.
[10] J. Gao, B. Li, X. Huang, L. Wang, L. Lin, H. Wang, H. Xue, *Chemical Engineering Journal*. **2019**, *373*.
[11] K. Tu, X. Wang, L. Kong, H. Guan, *Materials & Design*. **2018**, *140*.
[12] S. Alexander, J. Eastoe, A. M. Lord, F. d. r. Guittard, A. R. Barron, *ACS applied materials & interfaces*. **2016**, *8*.
[13] J. Sun, X. Li, J. Song, L. Huang, X. Liu, J. Liu, Z. Zhang, C. Zhao, *Journal of Dispersion Science and Technology*. **2018**, *39*.
[14] X. Zhang, J. Zhao, Q. Zhu, N. Chen, M. Zhang, Q. Pan, *ACS applied materials & interfaces*. **2011**, *3*.
[15] R. Weng, H. Zhang, L. Yin, W. Rong, Z. Wu, X. Liu, *RSC advances*. **2017**, *7*.
[16] C. Jiang, S. Xin, C. Wu, *AIP Advances*. **2011**, *1*.
[17] N. Wang, L. Tang, Y. Cai, W. Tong, D. Xiong, *Colloids and Surfaces A: Physicochemical and Engineering Aspects*. **2018**, *555*.
[18] T. Yamashita, P. Hayes, *Applied surface science*. **2008**, *254*.
[19] S. Huang, W. Zhang, S. Cui, W. Chen, L. Mi, *Inorganic Chemistry Frontiers*. **2017**, *4*.
[20] W. He, C. Wang, H. Li, X. Deng, X. Xu, T. Zhai, *Advanced Energy Materials*. **2017**, *7*.
[21] N. Kumar, K. Biswas, *Journal of Materials Research and Technology*. **2019**, *8*.
[22] F. A. Akgul, G. Akgul, N. Yildirim, H. E. Unalan, R. Turan, *Materials Chemistry and Physics*. **2014**, *147*.
[23] M. M. Can, S. I. Shah, M. F. Doty, C. R. Haughn, T. Fırat, *Journal of Physics D: Applied Physics*. **2012**, *45*.
[24] J. Zhu, B. Liu, L. Li, Z. Zeng, W. Zhao, G. Wang, X. Guan, *The Journal of Physical Chemistry A*. **2016**, *120*.
[25] N. Xu, D. K. Sarkar, X.-G. Chen, W. Tong, *Surface and Coatings Technology*. **2016**, *302*.
[26] S. L. Sanjay, B. G. Annaso, S. M. Chavan, S. V. Rajiv, *Journal of Surface Engineered Materials and Advanced Technology*. **2012**, *2012*.
[27] T. Steinmann, M. Arutkin, P. Cochard, E. Raphaël, J. Casas, M. Benzaquen, *Journal of Fluid Mechanics*. **2018**, *848*.

[28] H. Hu, J. Wen, L. Bao, L. Jia, D. Song, B. Song, G. Pan, M. Scaraggi, D. Dini, Q. Xue, *Science advances*. **2017**, *3*.
[29] C. Yu, M. Liu, C. Zhang, H. Yan, M. Zhang, Q. Wu, M. Liu, L. Jiang, *Giant*. **2020**.
[30] Y. Zhou, M. Li, B. Su, Q. Lu, *Journal of Materials Chemistry*. **2009**, *19*.
[31] F. J. Baldenebro-López, H. Camacho-Montes, A. Santos-Beltrán, M. C. Maldonado-Orozco, C. D. Gómez-Esparza, R. Martínez-Sánchez, *Materials Research*. **2016**, *19*.